

---

# Energy Dependent Intensity Variation of the Persistent X-ray Emission of Magnetars Observed with Suzaku

Yujin NAKAGAWA<sup>1</sup>, Ken EBISAWA<sup>2</sup> and Teruaki ENOTO<sup>3</sup>

<sup>1</sup>Center for Earth Information Science and Technology, Japan Agency for Marine-Earth Science and Technology, 3173-25 Showa-machi, Kanazawa-ku, Yokohama, Kanagawa 236-0001, Japan

<sup>2</sup>Institute of Space and Astronautical Science, Japan Aerospace Exploration Agency, 3-1-1 Yoshinodai, Chuo-ku, Sagamihara, Kanagawa 252-5210, Japan

<sup>3</sup>The Hakubi Center, Kyoto University, Yoshida-Ushinomiya-cho, Sakyo-ku, Kyoto 606-8501, Japan

\*E-mail: nakagawa.yujin@jamstec.go.jp, ebisawa.ken@jaxa.jp, enoto@kusastro.kyoto-u.ac.jp

Received 2017 May 18; Accepted

## Abstract

Emission mechanism of the magnetars is still controversial while various observational and theoretical studies have been made. In order to investigate mechanisms of both the persistent X-ray emission and the burst emission of the magnetars, we have proposed a model that the persistent X-ray emission consists of numerous micro-bursts of various sizes. If this model is correct, intensity Root Mean Square (RMS) variations of the persistent emission exceed the values expected from the Poisson distribution. Using *Suzaku* archive data of 11 magnetars (22 observations), the RMS intensity variations were calculated from 0.2 keV to 70 keV. As a result, we found significant excess RMS intensity variations from all the 11 magnetars. We suppose that numerous micro-bursts constituting the persistent X-ray emission cause the observed variations, suggesting that the persistent X-ray emission and the burst emission have identical emission mechanisms. In addition, we found that the RMS intensity variations clearly increase toward higher energy bands for 4 magnetars (6 observations). The energy dependent RMS

intensity variations imply that the soft thermal component and the hard X-ray component are emitted from different regions far apart from each other.

**Key words:** stars: magnetars — pulsars: general — X-rays: stars

---

## 1 Introduction

Magnetars are highly magnetized neutron stars (Duncan & Thompson 1992), and unique astrophysical objects to study physical phenomena under extremely high magnetic field strengths greater than the quantum critical level  $4.4 \times 10^{13}$  G (e.g., Lyne & Graham-Smith 2006). Among several classes of magnetars, soft gamma repeaters (SGRs) and anomalous X-ray pulsars (AXPs) are known to exhibit particularly intriguing X-ray emitting phenomena. While both exhibit persistent X-ray emission with typical luminosities of  $\sim 10^{34}$ – $10^{35}$  erg s $^{-1}$  in 2–10 keV, the SGRs and some AXPs occasionally exhibit sporadic short bursts with typical durations of  $\sim 100$  ms and luminosities of  $\sim 10^{39}$ – $10^{40}$  erg s $^{-1}$  in 2–100 keV. These unusual phenomena are thought to be caused by extremely strong magnetic field dissipation (Duncan & Thompson 1992).

Models which reproduce spectra of the persistent X-ray emission of the magnetars were studied based on observations by RXTE (Kuiper, Hermsen & Mendez 2004), INTEGRAL (Molkov et al. 2005; Rea et al. 2009) and *Suzaku* (Esposito et al. 2007; Nakagawa et al. 2009b; Enoto et al. 2010a; Enoto et al. 2010b; Enoto et al. 2010c; Enoto et al. 2017). These observational studies suggest that the magnetar persistent X-ray spectra consist of a soft thermal ( $< 10$  keV) component and a hard X-ray ( $> 10$  keV) component. The soft thermal component is reproduced by two blackbody functions (2BB) with typical temperatures of  $\sim 0.5$  keV and  $\sim 1.4$  keV, or a blackbody plus a power-law model (BB+PL) with a typical temperature of  $\sim 0.5$  keV and a typical power-law photon index of  $\sim 3$  (e.g., Nakagawa et al. 2009a). The hard X-ray component is well reproduced by a power-law model (PL) with a typical power-law photon index of  $\sim 1$  (e.g., Enoto et al. 2010c). The hard X-ray component should have a cutoff in high energy greater than  $\sim 200$  keV (e.g., Enoto et al. 2010b), otherwise the energy flux in the high energy goes to infinity. However, no clear evidence of the cutoff has been found (Li et al. 2017 for upper limits of gamma-ray emission in 0.1–10 GeV), while its hint has been reported (Yasuda et al. 2015).

Energy spectra of 50 short bursts from SGR 1806–20 and 5 short bursts from SGR 1900+14 with typical luminosities of  $\sim 10^{39}$ – $10^{40}$  erg s $^{-1}$  in 2–100 keV were observed by High Energy Transient Explorer 2 (HETE-2) with a wide energy band of 2–400 keV, and phenomenologically re-

produced by the 2BB model (Nakagawa et al. 2007) or the 2BB+PL model (Nakagawa et al. 2011). In recent studies based on *Suzaku* observations, energy spectra of weak bursts with luminosities of  $\sim 10^{36}$ – $10^{37}$  erg s $^{-1}$  in 2–40 keV from SGR 0501+4516 (Nakagawa, Makishima & Enoto 2011) and AXP 1E 1547.0–5408 (Enoto et al. 2012), which have lower luminosities than the typical short bursts, are reproduced with the hard X-ray component (PL) and the soft thermal component (2BB). Thus the energy spectra of the persistent X-ray emission, the typical short bursts and the weak bursts are likely to be reproduced by the same spectral model.

Several physical models have been proposed to explain emission mechanisms of the short bursts and the persistent X-ray emission. One of the ideas for the bursts is that the bursts are caused by heating of the magnetic corona due to local magnetic reconnections (Lyutikov 2003). The soft thermal component of the persistent X-ray emission is explained, e.g., by the Surface Thermal Emission and Magnetospheric Scattering (STEMS) model (Güver, Özel & Lyutikov 2006), the Resonant Cyclotron Scattering (RCS) model (Lyutikov & Gavriil 2006). Meanwhile, the hard X-ray component is explained by, e.g., thermal bremsstrahlung at the neutron star surface (Thompson & Beloborodov 2005; Beloborodov & Thompson 2007), Compton scattering in high magnetic fields (Baring & Harding 2007; Fernández & Thompson 2007), synchrotron emission in the magnetosphere (Heyl & Hernquist 2005b), a fallback disk model (Trümper et al. 2010) or a photon splitting model (Enoto et al. 2010c).

Based on the unified analysis of the persistent X-ray emission and the burst emission, two types of the correlation are reported: One is between the low and high temperatures of the 2BB components (2BB temperature correlation; Nakagawa et al. 2009a). The other is between the luminosities of the soft (2BB) and the hard (PL) components over five orders of magnitude (luminosity correlation; Nakagawa, Makishima & Enoto 2011).

Based on the unified spectral analysis, the 2BB temperature correlation, the luminosity correlation, and analogy with a relation between the solar microflare and the solar flare, we have proposed a new idea named "micro-burst model" that the persistent X-ray emission is composed of numerous micro-bursts of various sizes (Nakagawa et al. 2009a; Nakagawa, Makishima & Enoto 2011). The micro-bursts may have a duration much less than  $\sim 100$  ms, a typical duration of the short bursts. If the persistent X-ray emission is composed of such numerous micro-bursts, a cumulative number-intensity distribution of the micro-bursts would show a power-law distribution which has been found for typical short bursts (e.g., Nakagawa et al. 2007). Such power-law distribution is often referred to as the Gutenberg-Richter law (Gutenberg & Richter 1956).

We have calculated expected fluxes of the putative micro-bursts constituting the persistent X-ray emission by extrapolating the cumulative number-intensity distribution of typical bursts observed

by HETE-2 for SGR 1806–20 (Nakagawa et al. 2011). We found that the expected flux, accumulating the unresolved micro-bursts, is comparable to the observed persistent X-ray fluxes. A similar study was performed on an outburst of AXP 1E 1547.0–5408 with *Suzaku* (Enoto et al. 2012).

If the persistent X-ray emission is not static, but composed of numerous micro-bursts of various sizes following a particular cumulative number-intensity distribution, dispersion of the micro-burst intensities, as well as the persistent X-ray flux, should exceed the value expected from the Poisson distribution. In order to measure the dispersion quantitatively, in this paper, we calculate Root Mean Square (RMS) intensity variations in the persistent X-ray emission using the *Suzaku* data. *Suzaku* has great capabilities to estimate the RMS intensity variations, because the on-board narrow field instruments of X-ray imaging spectrometer (XIS; 0.2–12 keV; Koyama et al. 2007) and the hard X-ray detector (HXD; 10–700 keV; Takahashi et al. 2007) have high sensitivities and wide energy bands.

## 2 Observation and Data Reduction

The present studies are performed using *Suzaku* archive data of 11 magnetars (22 observations). Table 1 shows a summary of the observations. Besides, *Suzaku* archive data include the magnetars AXP Swift J1834.9–0846 and AXP 1E 1841–045, which are not used in the present study due to no significant detection and contamination by a nearby supernova remnant, respectively. Since there are not enough photon counts in the HXD-GSO energy band, we focus on the XIS and HXD-PIN data. Although HXD-PIN event data have a time resolution of 61  $\mu$ s, there are not enough photon counts to find any direct evidence of micro-bursts.

Reduction of the XIS and HXD-PIN event data were made using HEASoft 6.16 software. The latest calibration database (CALDB: 20150312) was applied to unfiltered XIS event data using *aepipeline* (v1.1.0). We created light curves and spectra from the cleaned XIS event data using *xselect* (v2.4c). Response matrix files were generated by *xisrmfgen* (v2012-04-21), and ancillary response function files by *xissimarfgen* (v2010-11-05). The net exposures of the XIS data are summarized in table 1.

The latest calibration database (CALDB: 20110915) was applied to unfiltered HXD-PIN event data using *aepipeline* (v1.1.0). We created light curves and spectra using *xselect*. Dead time corrections were applied to the spectra using *hxddtcor* (v1.50) as well as to the light curves using the recipe published on a *Suzaku* website<sup>1</sup>. Response matrix files were taken from CALDB<sup>2</sup>. The net exposures

<sup>1</sup> [http://www.astro.isas.jaxa.jp/suzaku/analysis/hxd/hxdfaq/hxd\\_dtcor\\_lc.html](http://www.astro.isas.jaxa.jp/suzaku/analysis/hxd/hxdfaq/hxd_dtcor_lc.html) (last accessed on 2017-10-16).

<sup>2</sup> We choose the response matrix files for each observation according to the instruction at <http://www.astro.isas.jaxa.jp/suzaku/analysis/hxd/pinnxb/quick/index.html>.

of the HXD-PIN data are summarized in table 1.

### 3 Data Analysis

For each observation, the XIS events were extracted from box regions centered on the objects, while the background events were extracted from box regions around the objects with the same area. The HXD-PIN background was subtracted using the background files supplied by Suzaku Guest Observer Facility<sup>3</sup>. The quoted errors hereafter refer to 68% confidence levels.

In this paper, we define the RMS intensity variations  $R$  as

$$R = \frac{[\frac{1}{N-1}\{\sum_i(x_i - \bar{x})^2 - \sum_i \delta_{x_i}^2\}]^{\frac{1}{2}}}{\bar{x}}, \quad (1)$$

where  $i$  is the bin number,  $x_i$  is the background-subtracted counts per bin,  $\bar{x}$  is the average of  $x_i$ ,  $\delta_{x_i}$  is the error of  $x_i$  and  $N$  is the number of bins. Here,  $N$  is obtained by dividing the net exposures in table 1 by the time bin-widths.

We calculated RMS intensity variations for each observation using the background-subtracted light curves in the 0.2–12 keV (XIS) and 10–70 keV (HXD-PIN) energy bands. Time resolutions of the light curves are 8 s in 0.2–12 keV and 128 s in 10–70 keV. The RMS intensity variations are found to be  $R_X = 1.3\text{--}135\%$  in the 0.2–12 keV energy band and  $R_P = 17\text{--}99\%$  in the 10–70 keV energy band, depending on sources and observations (table 1).

Based on Monte Carlo simulations, we confirmed that variations due to rotations of the magnetars ( $\sim 2\text{--}12$  s; e.g., Enoto et al. 2010c), and long-term ( $\sim 1$  day) flux variations do not affect the RMS intensity variations when using the 8 s (0.2–12 keV) light curves. We also estimated variations caused by background fluctuations using *Suzaku* data of hard and bright non-variable sources (table 2), and confirmed that the background fluctuations are not significant for most cases.

Next, we estimate effects of obviously bright bursts, which would significantly affect RMS intensity variations. We performed burst search using the 0.2–12 keV light curves with a 8 s time resolution of the XIS. We searched for such bright bursts in the light curves that exceed  $\lambda + 5\sigma$ , where  $\lambda$  is the average and  $\sigma$  is the standard deviation. Then we identified visually obvious bright bursts from 7 out of 22 observations as summarized in table 1. After removing the bright bursts from the light curves, we calculated the RMS variations as before. Consequently, the RMS intensity variations without influence of the bright burst emission are  $R'_X = 1.3\text{--}18.8\%$  in the 0.2–12 keV energy band and  $R'_P = 17\text{--}99\%$  in the 10–70 keV energy band as summarized in table 1. These variations are considered to be intrinsic variations of the persistent emission.

<sup>3</sup> <https://heasarc.gsfc.nasa.gov/docs/suzaku/analysis/pinbgd.html> (last accessed Oct 16, 2017)

We also calculated the RMS intensity variations with finer energy bands using the background-subtracted light curves of the XIS with a time resolution of 32 s. Figure 1 shows energy dependency of the RMS intensity variations with  $E^2 f(E)$  spectra where  $f(E)$  is the photon spectrum for each observation. The  $E^2 f(E)$  spectra are consistent with Enoto et al. (2017). Among the observations, the RMS intensity variations clearly increase toward higher energy bands for 4 magnetars (6 observations) as shown in the panels (a), (b), (d), (h), (m) and (o) in figure 1.

## 4 Result

### 4.1 Summary of Data Analysis

We calculated RMS intensity variations using the *Suzaku* data archive for 11 magnetars (22 observations). The RMS intensity variations are significantly greater than the values expected from the Poisson distribution for all the 22 observations of 11 magnetars in the 0.2–12 keV energy band (XIS) and 5 magnetars in the 10–70 keV energy band (HXD-PIN). For these 5 magnetars, there were 15 observations, and significant variation was detected from 8 out of them.

### 4.2 Mathematical Formulation of RMS Intensity Variations

In order to understand observed RMS intensity variations, we calculate expected RMS intensity variations with mathematical approach. We define the expected RMS intensity variations as

$$R_M = (\sigma_c^2 - \sigma_p^2)^{\frac{1}{2}} S_a^{-1}, \quad (2)$$

where  $\sigma_c^2$  is variance of the expected cumulative number-intensity distribution,  $\sigma_p^2$  is variance of Poisson distribution, and  $S_a$  is an average fluence of the micro-bursts. We assume that  $\sigma_c^2$ ,  $\sigma_p^2$  and  $S_a$  are defined as values in the 0.2–12 keV energy band. The expected RMS intensity variations are independent of the observation exposure time exceeding 1 ms, if we assume each micro-burst has 1 ms duration.

The expected cumulative number-intensity distribution from a single magnetar is defined as

$$N_c(> S_c) = A_c S_c^\alpha, \quad (3)$$

where  $A_c$  is a normalization,  $S_c$  is a fluence of micro-bursts,  $\alpha$  is an index, and  $N_c(> S_c)$  is a cumulative number of micro-bursts whose fluences are greater than  $S_c$ . The expected cumulative number-intensity distribution for a hypothetical magnetar is assumed to have  $\alpha = -1.1$  (Nakagawa et al. 2007) and  $A_c = 7 \times 10^{-9}$  bursts day $^{-1}$  at  $S_c = 1$  erg cm $^{-2}$ . A probability density function of the expected cumulative number-intensity distribution is defined as

$$\begin{aligned}
P(S_c) &= N'_c(> S_c) \left( \int_{S_1}^{S_2} N'_c(> S_c) dS_c \right)^{-1} \\
&= \frac{\alpha S_c^{\alpha-1}}{S_2^\alpha - S_1^\alpha},
\end{aligned} \tag{4}$$

where  $S_1$  and  $S_2$  ( $S_1 < S_2$ ) are minimum and maximum fluences of the interval of  $S_c$  which satisfy the probability density function. Using equation (4), variance of the expected cumulative number-intensity distribution is calculated as

$$\begin{aligned}
\sigma_c^2 &= E[S_c^2] - (E[S_c])^2 \\
&= \int_{S_1}^{S_2} S_c^2 P(S_c) dS_c - \left\{ \int_{S_1}^{S_2} S_c P(S_c) dS_c \right\}^2 \\
&= -\alpha A_c f_m^{-1} \int_{S_1}^{S_2} S_c^{\alpha+1} dS_c - \left\{ \alpha A_c f_m^{-1} \int_{S_1}^{S_2} S_c^\alpha dS_c \right\}^2 \\
&= \begin{cases} \frac{\alpha}{\alpha+2} A_c f_m^{-1} (S_1^{\alpha+2} - S_2^{\alpha+2}) - \left\{ \frac{\alpha}{\alpha+1} A_c f_m^{-1} (S_1^{\alpha+1} - S_2^{\alpha+1}) \right\}^2 & (\alpha \neq -1 \wedge 0 > \alpha > -2) \\ A_c f_m^{-1} (S_1 - S_2) - \{ A_c f_m^{-1} (\log |S_1| - \log |S_2|) \}^2 & (\alpha = -1) \end{cases} \tag{5}
\end{aligned}$$

where  $E[S_c^2]$  is an expectation of  $S_c^2$ ,  $E[S_c]$  is an expectation of  $S_c$  and  $f_m = -A_c(S_2^\alpha - S_1^\alpha)$  is a frequency of the micro-bursts with the fluences between  $S_1$  and  $S_2$ . Variance of the expected cumulative number-intensity distribution  $\sigma_c^2$  depends on the frequency of micro-bursts  $f_m$  as well as the fluence distribution index  $\alpha$ . Hence, the values of  $R_M$  depend on choices of  $S_1$ ,  $S_2$  and  $\alpha$ . Figure 2 (left) shows a two-dimensional contour graph of  $R_M$  with respect to  $S_1$  and  $S_2$ , and figure 2 (right) shows a relation between  $\alpha$  and  $R_M$ ; other parameter values are fixed to those determined below.

Short bursts are known to have spiky structures in 0.5 ms light curves, which may be caused by a rapid energy reinjection and cooling (Nakagawa et al. 2007). We assume 1 ms durations for the micro-bursts under the assumption that one cycle of the energy reinjection and cooling corresponds to a single micro-burst. Using the assumed duration of 1 ms for the micro-bursts and typical flux of  $10^{-11} \text{ erg cm}^{-2} \text{ s}^{-1}$  for the persistent X-ray emission, we assume  $S_1 = 0.001 \text{ s} \times 10^{-11} \text{ erg cm}^{-2} \text{ s}^{-1} = 10^{-14} \text{ erg cm}^{-2}$ . We also assume  $S_2 = 10^{-11} \text{ erg cm}^{-2}$  which is substantially below a burst detection limit of *Suzaku* ( $5\sigma \approx 10^{-10} \text{ erg cm}^{-2}$  described in section 3). We found  $\sigma_c^2 = 5.8 \times 10^{-26} \text{ erg}^2 \text{ cm}^{-4}$  from equation (5).

The expected cumulative Poisson distribution is defined as  $N_p(> k') = A_p(1 - e^{-\lambda} \sum_{k=0}^{k'} \lambda^k / k!)$ , where  $A_p$  is a normalization,  $\lambda$  is mean counts per bin of a light curve,  $k'$  and  $k$  are integer values, and  $N_p(> k')$  is a cumulative number of the bins corresponding to micro-bursts for which  $k$  is greater than  $k'$ . The expected cumulative Poisson distribution for the hypothetical magnetar has  $\lambda = 12.12 \text{ counts} (2\text{s})^{-1}$  in the 0.2–12 keV energy band (Nakagawa, Makishima & Enoto 2011) and an assumed normalization of  $A_p = 2 \times 10^5 \text{ bursts day}^{-1}$ . We assume that

$\lambda = 12.12 \text{ counts } (2\text{s})^{-1}$  correspond to an average fluence of the micro-bursts in the 0.2–12 keV energy band of  $S_a = 7.54 \times 10^{-13} \text{ erg cm}^{-2}$ . We also assume that  $k'$  has a fluence  $S_p(k')$  where  $S_p(k'+1) - S_p(k') = S_p(1) = \lambda^{-1} S_a$  is  $6.22 \times 10^{-14} \text{ erg cm}^{-2}$ . We found the variance of the expected Poisson distribution as  $\sigma_p^2 = \lambda^{-1} S_a^2 = 4.7 \times 10^{-26} \text{ erg}^2 \text{ cm}^{-4}$ .

Finally, we obtain  $R_M = 14\%$  for the hypothetical magnetar by substituting  $\sigma_c^2$ ,  $\sigma_p^2$  and  $S_a$  shown above in equation (2). This is consistent with the observed values of  $R'_X = 1.3\text{--}18.8\%$ . Difference of the RMS intensity variations among magnetars may be explained by difference of the fluence distribution index  $\alpha$ .

### 4.3 Comparison of cumulative number-intensity distributions

Figure 3 shows comparison between the expected cumulative number-intensity distribution of the micro-bursts and that expected from Poisson distribution for a hypothetical magnetar. We see that the former clearly has a wider distribution than the latter. In particular, reduction of the bursts above  $\sim 2 \times 10^{-12} \text{ erg cm}^{-2}$  makes the expected cumulative number-intensity distribution closer to that expected from Poisson distribution. We confirmed that the RMS intensity variations significantly exceed the values expected from the Poisson distribution even after removing bright bursts (section 3). The wider cumulative number-intensity distribution can naturally explain the observed excess RMS intensity variations. Thus, the observation is consistent with the assumption that the persistent X-ray emission is composed of numerous micro-bursts of various sizes subject to a particular cumulative number-intensity distribution.

## 5 Discussion

### 5.1 Expected Flux from Cumulative Number-Intensity Distribution

Integrating energies of the micro-bursts from  $S_c = 10^{-14} \text{ erg cm}^{-2}$  to  $10^{-11} \text{ erg cm}^{-2}$  using the expected cumulative number-intensity distribution in section 4.2 (Nakagawa et al. 2007), we obtain the persistent X-ray flux of a hypothetical magnetar as  $\sim 1.1 \times 10^{-11} \text{ erg cm}^{-2} \text{ s}^{-1}$ . This is comparable with a typical observed flux of  $\sim 9.9 \times 10^{-12} \text{ erg cm}^{-2} \text{ s}^{-1}$  for SGR 1806–20 (Nakagawa et al. 2009b). This result is consistent with the persistent X-ray fluxes estimated from observed cumulative number-intensity distributions obtained by Nakagawa et al. (2011) and Enoto et al. (2012).

### 5.2 Energy Dependent RMS Intensity Variations

We discovered that energy dependencies of the RMS intensity variations for 4 magnetars (6 observations; panels (a), (b), (d), (h), (m) and (o) in figure 1), clearly increase toward higher energy bands.

Among these observations, the RMS intensity variations remarkably increase above  $\sim 8$  keV and  $\sim 4$  keV for SGR 0501+4516 (OBSID=404078010; panel (a) in figure 1) and AXP 1E 1547.0–5408 (OBSID=903006010; panel (m) in figure 1), respectively. These energies correspond to the crossing points of the soft thermal components and the hard X-ray components, suggesting that the most variation is associated with the hard components.

The energy dependent RMS intensity variations may be explained by the micro-burst model presented in section 4.2. It is reported that indices of the cumulative number-intensity distribution of short bursts increase toward higher energy bands in SGR 1806–20 (Nakagawa et al. 2007). Increase of the index causes a high dispersion of fluences, which leads to a large RMS intensity variation as shown in figure 2 (right). If the same energy dependence of the index is applicable to the micro-bursts, smaller RMS intensity variation in lower energy bands is caused by smaller indices, and vice versa.

### 5.3 Comparison with Theoretical Models

The present results will give constraints on persistent X-ray emission mechanisms of the magnetars. Significant RMS intensity variations in both the 0.2–12 keV energy band and the 10–70 keV energy band imply that neither the soft thermal component nor the hard X-ray component is from the stable neutron star surface in thermal equilibrium. In this context, thermal bremsstrahlung model at the neutron star surface (Thompson & Beloborodov 2005; Beloborodov & Thompson 2007) is unlikely.

Energy dependence of the RMS intensity variations suggests that the emission regions of the soft thermal component and the hard X-ray component are located separately. In the magnetospheric synchrotron model (Heyl & Hernquist 2005b), the soft thermal component is emitted from a fireball near the neutron star and the hard X-ray component is emitted via synchrotron process far from the neutron star. Thus, this model seems consistent with the present result of the energy dependent RMS intensity variations. In fact, power-law indices of the hard X-ray components expected from the synchrotron model (0.5; Heyl & Hernquist 2005b) is comparable to the observed indices (0.3–1.7; Enoto et al. 2010c). Furthermore, the synchrotron model is applicable not only to the persistent emission but also to the burst emissions (Heyl & Hernquist 2005a). This agrees with our idea that the persistent X-ray emission is composed of numerous micro-bursts, and that the persistent emission and the burst emission have the same origin.

### 5.4 A Unified View of the Magnetar X-ray Emission

Figure 4 shows a schematic illustration of our unified view (“Micro-Burst Model”) of both the persistent X-ray emission and the burst emission from magnetars, based on the present observation

and theoretical models (Duncan & Thompson 1992; Thompson & Duncan 1995; Heyl & Hernquist 2005a; Heyl & Hernquist 2005b). In this model, the burst emission is caused by a single energetic fireball, while the persistent X-ray emission consists of numerous micro-bursts caused by numerous small fireballs. In the unified view, both the persistent X-ray emission and the burst emission are explained under the same configuration, where only their luminosities are different. The persistent X-ray emission and the burst emission have typical luminosities of  $\sim 10^{35}$  erg s $^{-1}$  and  $\sim 10^{37}$  –  $\sim 10^{40}$  erg s $^{-1}$ , respectively (e.g., Nakagawa, Makishima & Enoto 2011).

Initially, a starquake occurs on the magnetar surface (Duncan & Thompson 1992; process 1 in figure 4). The starquake produces an electron-positron pair plasma fireball which has momenta to leave from the magnetar. The fireball travels in the magnetosphere and emits blackbody emissions (i.e., the soft-thermal components) at around  $\sim 100R_{\text{NS}}$  where  $R_{\text{NS}}$  is a typical neutron star radius of  $\sim 10$  km (Heyl & Hernquist 2005b; process 2 in figure 4). The emissions is observed as two blackbody spectra, because of two different polarization modes in strong magnetic fields of  $\sim 10^{14}$  G (Thompson & Duncan 1995). Their typical temperatures are  $\sim 0.5$  keV and  $\sim 1.4$  keV for the persistent X-ray emission (e.g., Nakagawa et al. 2009a), or  $\sim 4$  keV and  $\sim 11$  keV for the burst emission (e.g., Nakagawa et al. 2007).

Eventually, the fireball turns to optically thin condition and emits synchrotron emissions (i.e., the hard X-ray components) at around  $\sim 1000R_{\text{NS}}$  (Heyl & Hernquist 2005b; process 3 in figure 4). The spatial scale of causality for the hard X-ray components is estimated to be  $\sim 30R_{\text{NS}}$  in assuming that the micro-burst has 1 ms duration. Therefore the size of each fireball should be less than  $\sim 30R_{\text{NS}}$ . Number of the electrons to produce the hard X-ray component for the persistent X-ray emission may be lower by 2–3 orders of magnitude than that for the burst emission (Nakagawa, Makishima & Enoto 2011). Presumably, the magnetic disturbance is increased outward from the magnetars, so that the strong magnetic disturbance causes the larger RMS intensity variations in the hard X-ray components.

## 6 Conclusion

Using the *Suzaku* archive data of 11 magnetars (22 observations), we found significant RMS intensity variations in the persistent X-ray emission from all the magnetars studied. In addition, we found that the RMS intensity variations increase toward higher energy band for 4 magnetars (6 observations). These RMS intensity variations are consistent with the micro-burst model, where the persistent X-ray emission is composed of numerous micro-bursts of various sizes subject to a particular cumulative number-intensity distribution. We propose a unified view of the magnetar X-ray emission based on the present results.

Time scale of the flux variations expected in the micro-burst model is shorter than a few milliseconds (Nakagawa et al. 2007). Future observations of magnetars with a higher sensitivity and better time resolution, which is expected to give more accurate measurements of the RMS intensity variations will allow us to strongly constrain magnetar emission mechanisms by directly comparing with theoretical models (e.g., Duncan & Thompson 1992; Thompson & Duncan 1995; Heyl & Hernquist 2005a; Heyl & Hernquist 2005b).

## **Acknowledgments**

This work was supported by JSPS KAKENHI Grant Numbers 24540309, 15K05117 and 16K05309.

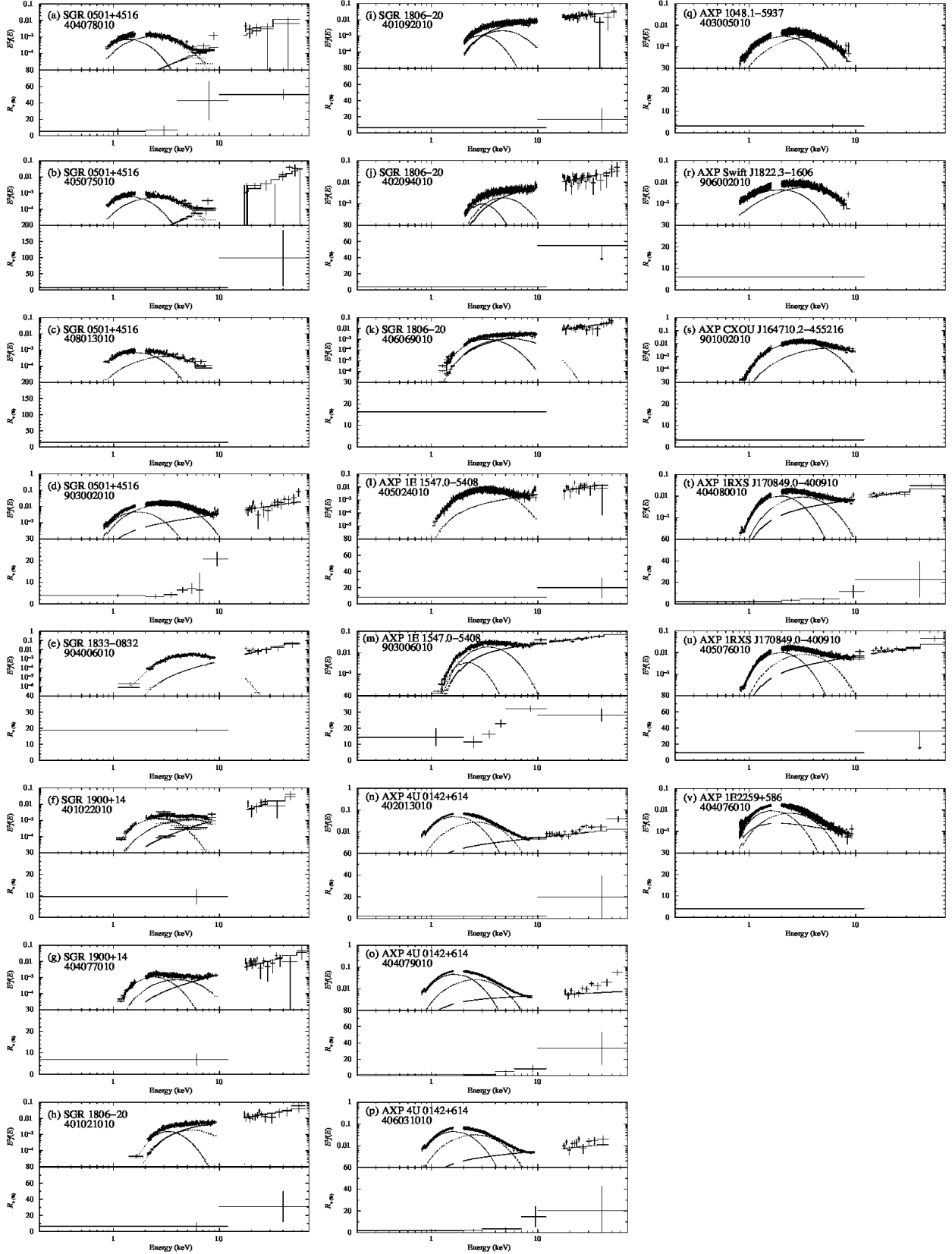
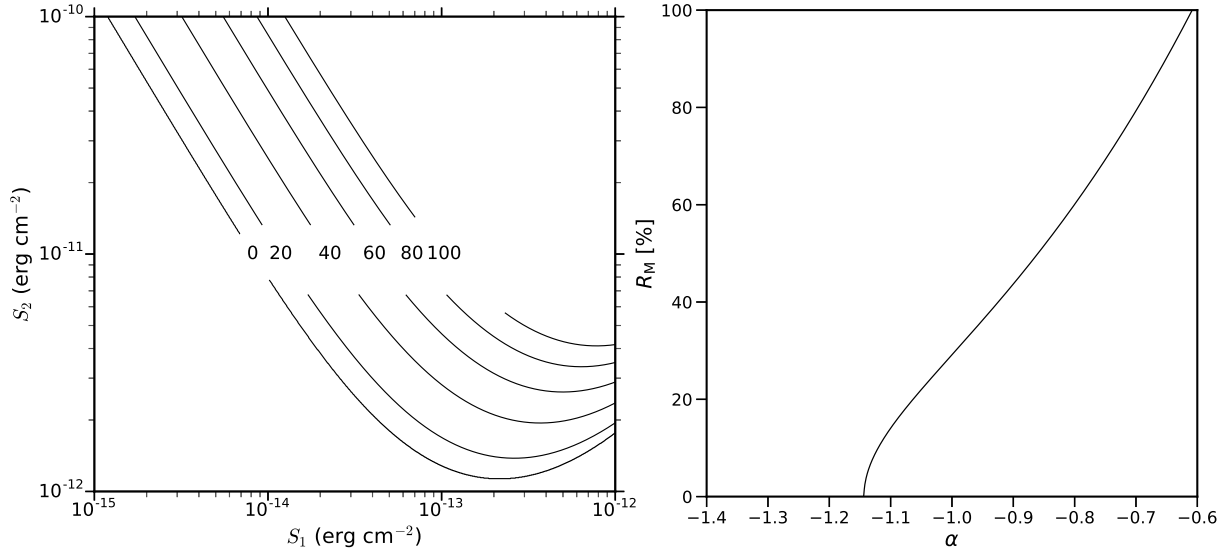
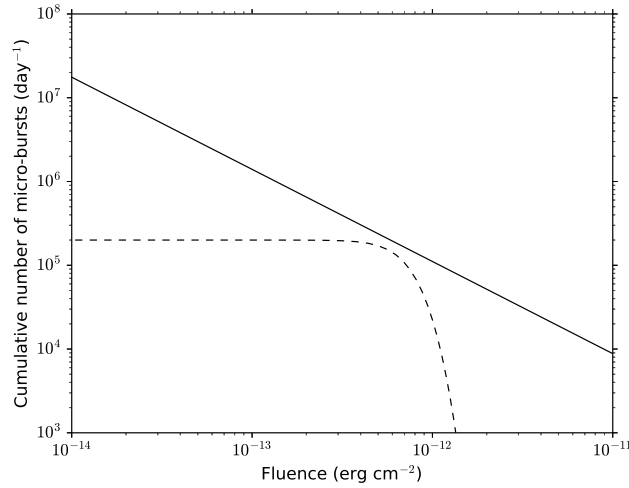


Fig. 1.  $E^2 f(E)$  spectra, and spectra of the RMS intensity variations. The spectra in the panels (c), (q), (r), (s) and (v) are fitted with 2BB. The spectrum in the panel (e) is fitted with BB+PL. The spectra in the other panels are fitted with 2BB+PL.



**Fig. 2.** Left: A two-dimensional contour graph of  $R_M$  with respect to  $S_1$  and  $S_2$ . Contour lines are plotted for  $R_M$  ranging from 0 to 100. Right: A relation between  $\alpha$  and  $R_M$ .



**Fig. 3.** An expected cumulative number-intensity distribution of the micro-bursts (solid line) and an assumed cumulative Poisson distribution (dashed line). See details in text.

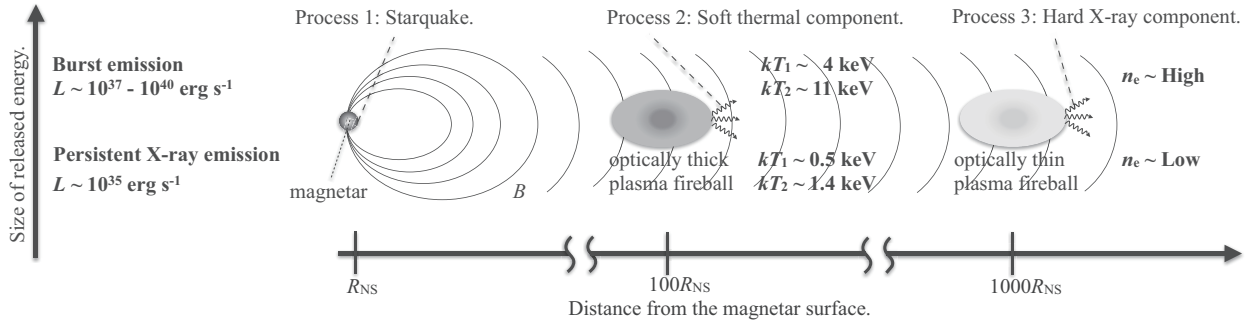


**Fig. 4.** A schematic illustration of our "Micro-Burst Model" of both the persistent X-ray emission and the burst emission from magnetars.  $R_{NS}$  indicates a typical neutron star radius of  $\sim 10$  km,  $L$  indicates a typical luminosity,  $kT_1$  and  $kT_2$  indicate typical blackbody temperatures and  $n_e$  indicates number of electrons in emission regions. Magnetic disturbance may be strong at a distance of  $\sim 1000R_{NS}$  and may cause the large RMS intensity variations.

**Table 1.** Summary of magnetars used in this study and their RMS intensity variations.

Object*	OBSID <sup>†</sup>	Date <sup>‡</sup> (UTC)	$T_X$ <sup>§</sup> (ks)	$T_P$ <sup>§</sup> (ks)	$N_b$ <sup>  </sup>	$R_X$ <sup>#</sup> (%)	$R_P$ <sup>**</sup> (%)	$R'_X$ <sup>††</sup> (%)	$R'_P$ <sup>‡‡</sup> (%)
SGR 0501+4516	404078010	2009-08-17	43	25	0	9.2±1.1	50 ± 6	9.2±1.1	50 ± 6
	405075010	2010-09-20	60	49	0	7.2±2.5	99 ± 86	7.2±2.5	99 ± 86
	408013010 <sup>§§</sup>	2013-08-31	41	33	0	14±1	—	14±1	—
	903002010	2008-08-26	60	50	17	50.9±0.5	0	7.37±0.07	0
SGR 1833–0832	904006010	2010-03-27	42	10	2	27.5±0.7	0	18.8±1.1	0
SGR 1900+14	401022010	2006-04-01	22	13	0	6.8±2.7	0	6.8±2.7	0
	404077010	2009-04-26	53	39	0	9.6±3.5	0	9.6±3.5	0
SGR 1806–20	401021010	2007-03-30	19	16	2	51±1	26±24	6.4±4.8	31 ± 19
	401092010	2006-09-09	49	52	9	135±1	59±5	6.5±0.8	17 ± 13
	402094010	2007-10-14	52	46	6	82.7±0.9	75±7	4.2±0.5	< 55
	406069010	2012-03-24	71	60	0	16.4±0.4	0	16.4±0.4	0
AXP 1E 1547.0–5408	405024010	2010-08-07	52	40	0	8.4±0.6	20 ± 12	8.4±0.6	20 ± 12
	903006010	2009-01-28	11	31	25	36.0±0.3	32±3	18.2±0.2	28 ± 3
AXP 4U 0142+614	402013010	2007-08-13	100	95	0	2.0±0.1	< 40	2.0±0.1	< 40
	404079010	2009-08-10	107	92	0	1.3±0.3	33 ± 20	1.3±0.3	33 ± 20
	406031010	2011-09-07	39	39	0	1.8±0.3	< 42	1.8±0.3	< 42
AXP 1E 1048.1–5937	403005010 <sup>§§</sup>	2008-11-30	100	63	1	3.0±1.0	—	3.0±1.0	—
AXP Swift J1822.3–1606	906002010 <sup>§§</sup>	2011-09-13	41	34	0	6.0±0.3	—	6.0±0.3	—
AXP CXOU J164710.2–455216	901002010 <sup>   </sup>	2006-09-23	39	—	0	3.3±0.7	—	3.3±0.7	—

\* Object name of the SGRs and AXPs.

<sup>†</sup> *Suzaku* observation ID.

<sup>‡</sup> Date of the observation start.

<sup>§</sup> Net exposures of the XIS ( $T_X$ ) and the HXD-PIN ( $T_P$ ).

<sup>||</sup> Number of bins where photon counts exceed a burst criteria. See details in text.

<sup>#</sup> The RMS intensity variations in 0.2–12 keV (XIS).

<sup>\*\*</sup> The RMS intensity variations in 10–70 keV (HXD-PIN).

<sup>††</sup> The RMS intensity variations without effect of the burst emission in 0.2–12 keV (XIS).

<sup>‡‡</sup> The RMS intensity variations without effect of the burst emission in 10–70 keV (HXD-PIN).

<sup>§§</sup> The HXD-PIN data did not show a statistically significant signal.

<sup>|||</sup> The HXD-PIN data was not used due to a contamination source in a field of view.

**Table 1.** (Continued)

Object*	OBSID <sup>†</sup>	Date <sup>‡</sup> (UTC)	$T_X$ <sup>§</sup> (ks)	$T_P$ <sup>§</sup> (ks)	$N_b$ <sup>  </sup>	$R_X$ <sup>#</sup> (%)	$R_P$ <sup>**</sup> (%)	$R'_X$ <sup>††</sup> (%)	$R'_P$ <sup>‡‡</sup> (%)
AXP 1RXS J170849.0–400910	404080010	2009-08-23	61	48	0	$7.85 \pm 0.07$	$23 \pm 16$	$7.85 \pm 0.07$	$23 \pm 16$
	405076010	2010-09-27	63	55	0	$9.25 \pm 0.06$	< 36	$9.25 \pm 0.06$	< 36
AXP 1E 2259+586	404076010 <sup>§§</sup>	2009-05-25	123	96	0	$4.1 \pm 0.1$	–	$4.1 \pm 0.1$	–

\* Object name of the SGRs and AXPs.

<sup>†</sup> *Suzaku* observation ID.

<sup>‡</sup> Date of the observation start.

<sup>§</sup> Net exposures of the XIS ( $T_X$ ) and the HXD-PIN ( $T_P$ ).

<sup>||</sup> Number of bins where photon counts exceed a burst criteria. See details in text.

<sup>#</sup> The RMS intensity variations in 0.2–12 keV (XIS).

<sup>\*\*</sup> The RMS intensity variations in 10–70 keV (HXD-PIN).

<sup>††</sup> The RMS intensity variations without effect of the burst emission in 0.2–12 keV (XIS).

<sup>‡‡</sup> The RMS intensity variations without effect of the burst emission in 10–70 keV (HXD-PIN).

<sup>§§</sup> The HXD-PIN data did not show a statistically significant signal.

<sup>|||</sup> The HXD-PIN data was not used due to a contamination source in a field of view.

## **Appendix. RMS Intensity Variations Caused by Background Fluctuations**

Suzaku data of hard and bright non-variable sources (table 2) are analyzed, in order to estimate the RMS intensity variations caused by background fluctuations and their time dependencies. The RMS intensity variations are found to be  $R_X = 0.8\text{--}2.5\%$  in the 0.2–12 keV energy band and  $R_P = 5\text{--}12\%$  in the 10–70 keV energy band, depending on observation periods. We found that the time dependency is marginal and confirmed that the background fluctuations are not significant for most cases.

**Table 2.** Summary of objects used for the background fluctuations and their RMS intensity variations.

Object*	OBSID <sup>†</sup>	Date <sup>‡</sup> (UTC)	$T_X$ <sup>§</sup> (ks)	$T_P$ <sup>§</sup> (ks)	$R_X$ <sup>  </sup> (%)	$R_P$ <sup>#</sup> (%)
Cas A <sup>††</sup>	100016010**	2005-09-01	–	24	–	12±5
	100043010 <sup>‡‡</sup>	2006-02-02	–	10	–	< 40
	100043020	2006-02-17	7	16	0.8±0.5	< 26
	507038010	2012-12-20	102	118	1.56±0.02	< 28
Coma Cluster	801097010	2006-05-31	179	157	0.8±0.3	5±4
Perseus Cluster <sup>††</sup>	101012020	2007-02-05	44	42	< 1.6	6±5
	102011010	2007-08-15	42	36	0.9±0.7	7±5
	102012010	2008-02-27	42	62	0.9±0.7	7±3
	103004010	2008-08-13	41	32	1.5±0.3	0
	103004020	2009-02-11	50	45	1.2±0.4	< 16
	103005010	2008-08-14	21	17	< 12	< 386
	103005020	2009-02-12	29	27	< 6	0
	104018010	2009-08-26	41	37	1.1±0.5	< 46
	104019010	2010-02-01	39	36	1.7±0.3	< 173
	104020010	2009-08-27	55	52	1.2±0.3	< 20
	104021010	2010-02-02	22	22	< 4	< 31
	105009010	2010-08-09	34	38	0.9±0.8	0
	105009020	2011-02-03	40	30	1.3±0.4	< 16
105010010	2010-08-10	27	34	< 2	< 20	

\* Object name.

<sup>†</sup> *Suzaku* observation ID.

<sup>‡</sup> Date of the observation start.

<sup>§</sup> Net exposures of the XIS ( $T_X$ ) and the HXD-PIN ( $T_P$ ).

<sup>||</sup> The RMS intensity variations in 0.2–12 keV (XIS).

<sup>#</sup> The RMS intensity variations in 10–70 keV (HXD-PIN).

\*\* The XIS data was not used due to a telemetry saturation (Maeda et al. 2009).

<sup>††</sup> The data of OBSID=508011020 for Cas A and OBSID=101012010 for Perseus Cluster were not used due to visually obvious flux variations in light curves.

<sup>‡‡</sup> The XIS data was not available.

<sup>§§</sup> The HXD-PIN data was not available.

**Table 2.** (Continued)

Object*	OBSID <sup>†</sup>	Date <sup>‡</sup> (UTC)	$T_X$ <sup>§</sup> (ks)	$T_P$ <sup>§</sup> (ks)	$R_X$ <sup>  </sup> (%)	$R_P$ <sup>#</sup> (%)
	105010020	2011-02-02	21	17	< 3	< 21
	105027010	2011-02-22	46	42	1.7±0.2	11±3
	105028010	2011-02-21	21	18	1.3±1.2	0
	106005010	2011-07-27	41	37	< 6.4	< 412
	106005020	2012-02-07	47	45	1.2±0.4	0
	106006010	2011-07-26	40	35	0.9±0.8	0
	106007010	2011-08-23	21	19	1.3±0.8	0
	106007020	2012-02-08	21	21	< 3	10±7
	106008010	2011-08-22	23	22	< 2	< 19
	107005010	2012-08-20	41	39	0.9±0.6	12±3
	107005020	2013-02-11	41	36	1.1±0.6	0
	107006010	2012-08-20	24	20	< 2	9±7
	107006020	2013-02-12	22	18	2.0±0.4	10±6
	108005010	2013-08-15	41	41	1.2±0.4	< 38
	108005020 <sup>§§</sup>	2014-02-05	38	—	1.2±0.5	—
	108006010	2013-08-16	22	19	1.2±0.8	< 20
	108006020 <sup>§§</sup>	2014-02-06	19	—	< 2	—
	109005010 <sup>§§</sup>	2014-08-27	20	—	< 3.5	—
	109005020 <sup>§§</sup>	2015-03-03	37	—	1.4±0.3	—
	109006010 <sup>§§</sup>	2015-03-04	24	—	2.5±0.4	—

\* Object name.

<sup>†</sup> *Suzaku* observation ID.

<sup>‡</sup> Date of the observation start.

<sup>§</sup> Net exposures of the XIS ( $T_X$ ) and the HXD-PIN ( $T_P$ ).

<sup>||</sup> The RMS intensity variations in 0.2–12 keV (XIS).

<sup>#</sup> The RMS intensity variations in 10–70 keV (HXD-PIN).

\*\* The XIS data was not used due to a telemetry saturation (Maeda et al. 2009).

<sup>††</sup> The data of OBSID=508011020 for Cas A and OBSID=101012010 for Perseus Cluster were not used due to visually obvious flux variations in light curves.

<sup>‡‡</sup> The XIS data was not available.

<sup>§§</sup> The HXD-PIN data was not available.

**Table 2.** (Continued)

Object*	OBSID <sup>†</sup>	Date <sup>‡</sup>	$T_X$ <sup>§</sup>	$T_P$ <sup>§</sup>	$R_X$ <sup>  </sup>	$R_P$ <sup>#</sup>
		(UTC)	(ks)	(ks)	(%)	(%)
	109007010 <sup>§§</sup>	2015-03-05	31	—	1.2±0.8	—

\* Object name.

<sup>†</sup> *Suzaku* observation ID.

<sup>‡</sup> Date of the observation start.

<sup>§</sup> Net exposures of the XIS ( $T_X$ ) and the HXD-PIN ( $T_P$ ).

<sup>||</sup> The RMS intensity variations in 0.2–12 keV (XIS).

<sup>#</sup> The RMS intensity variations in 10–70 keV (HXD-PIN).

\*\* The XIS data was not used due to a telemetry saturation (Maeda et al. 2009).

<sup>††</sup> The data of OBSID=508011020 for Cas A and OBSID=101012010 for Perseus Cluster were not used due to visually obvious flux variations in light curves.

<sup>‡‡</sup> The XIS data was not available.

<sup>§§</sup> The HXD-PIN data was not available.

## References

- Baring, M.G., & Harding, A.K. 2007, *Ap&SS*, 308, 109-118
- Beloborodov, A.M., & Thompson, C. 2007, *Ap&SS*, 308, 631-639
- Dennis, B. R. 1985, *Sol. Phys.*, 100, 465
- Duncan, R.C., & Thompson, C. 1992, *ApJ*, 392, L9-L13
- Enoto, T. et al. 2010a, *ApJ*, 715, 665-670
- Enoto, T. et al. 2010b, *PASJ*, 62, 475-485
- Enoto, T. et al. 2010c, *ApJ*, 722, L162-L167
- Enoto, T. et al. 2012, *MNRAS*, 427, 2824-2840
- Enoto, T. et al. 2017, *ApJS*, accepted
- Esposito, P. et al. 2007, *A&A*, 476, 321-330
- Ferández, R., & Thompson, C. 2007, *ApJ*, 660, 615-640
- Gavriil, F.P., & Kaspi, V.M. 2004, *ApJ*, 609, L67-L70
- Götz, D. et al. 2006, *A&A*, 445, 313-321
- Gutenberg, B., & Richter, C.F. 1956, *Annals of Geophysics*, 9, pp.1-15
- Güver, T., Özel, F., & Lyutikov, M. 2006, *arXiv:astro-ph/0611405*
- Heyl, J.S., & Hernquist, L. 2005a, *ApJ*, 618, 463-473
- Heyl, J.S., & Hernquist, L. 2005b, *MNRAS*, 362, 777-783
- Kagan, Y. Y. 1999, *Pure Appl. Geophys.*, 155, 537
- Koyama, K. et al. 2007, *PASJ*, 59, 23-33
- Kuiper, L., Hermsen, W., & Mendez, M. 2004, *ApJ*, 613, 1173-1178
- Li, J., Rea, N., Torres, F.D., & de Oña-Wilhelmi, E., *ApJ*, 835, 30 (10pp)
- Lin, L., Göğüş, E., Kaneko Y., & Kouveliotou C. 2013, *ApJ*, 778, 105 (11pp)
- Lyne, A., & Graham-Smith, F. 2006, *Cambridge Astrophysics Series*, 38, 149
- Lyutikov, M. 2003, *MNRAS*, 346, 540-554
- Lyutkov, M., & Gavriil F.P. 2006, *MNRAS*, 368, 690-706
- Maeda, Y. et al. 2009, *PASJ*, 61, 1217-1228
- Molkov, S. et al. 2005, *A&A*, 433, L13-L16
- Nakagawa, Y.E. et al. 2007, *PASJ*, 59, 653-678
- Nakagawa, Y.E., Yoshida, A., Yamaoka, K., & Shibazaki, N. 2009, *PASJ*, 61, 109-122
- Nakagawa, Y.E. et al. 2009, *PASJ*, 61, S387-S393
- Nakagawa, Y.E., Makishima, K., & Enoto, T. 2011, *PASJ*, 63, S813-S820
- Nakagawa, Y.E., Enoto, T., Makishima, K., Yoshida, A., Yamaoka, K., Sakamoto, T., Rea, N., & Hurley, K.

- 2011, High-Energy Emission from Pulsars and their Systems, Astrophysics and Space Science Proceedings (Berlin: Springer-Verlag Berlin Heidelberg), 323-327
- Olive, J.-F., Hurley, K., Sakamoto, T., Atteia, J.-L., Crew, G., Ricker, G., Pizzichini, G., & Barraud, C. 2004, ApJ, 616, 1148-1158
- Rea, N. et al. 2009, MNRAS, 396, 2419-2432
- Takahashi, T. et al. 2007, PASJ, 59, 35-51
- Takahashi, T., Mitsuda, K., Kelley, R., Fabian, A., Mushotzky, R., Ohashi, T., & Petre, R. on behalf of the ASTRO-H Science Working Group 2014, arXiv: astro-ph/1412.2351
- Thompson, C., & Beloborodov, A.M. 2005, ApJ, 634, 565-569
- Thompson, C., & Duncan, R.C. 1995, MNRAS, 275, 255-300
- Trümper, J.E., Zezas, A., Ertan, Ü, & Kylafis, N.D. 2010, A&A, 518, A46 (1-5)
- Yasuda, T. et al. 2015, PASJ, 67, 41 (1-12)